FST16-129: Tritium 2016 Abstract #16789

Cavity formation in molybdenum studied *in situ* in the TEM

D.C. Bufford[1], C.S. Snow[1], and K. Hattar[1*]

[1]*Sandia National Laboratories, Albuquerque, NM, USA*

Daniel Bufford: dcbuffo@sandia.gov

Clark Snow: cssnow@sandia.gov

[*]Khalid Hattar: khattar@sandia.gov, corresponding author

P.O. Box 5800
Albuquerque, NM, USA 87185

Phone: 505.845.9859

Fax: 505.844.7775

Pages: 15

Tables: 0

Figures: 4

Cavity formation in molybdenum studied *in situ* in the TEM

D.C. Bufford[1], C.S. Snow[1], and K. Hattar[1*]

[1]*Sandia National Laboratories, Albuquerque, NM, USA*

Abstract:

We investigated the microstructural response of molybdenum, with and without prior exposure to gaseous deuterium, during helium irradiation and subsequent annealing. Ion irradiations and annealing experiments were performed *in situ* in a transmission electron microscope, enabling real time observation of the microstructural evolution. Cavities approximately 0.5 nm in diameter were formed in deuterium-exposed molybdenum at a fluence of 1.7×10^{15} helium cm^{-2}, but did not grow appreciably after increasing the fluence by two orders of magnitude or after brief room temperature aging. Similar cavities were not apparent in pristine molybdenum. Larger cavities appeared in both samples during *in situ* annealing to 1063 K, without any clear differences between the two samples. The evolving cavity morphologies are discussed in terms of defect production, microstructure, and sample geometry.

Keywords: Cavities; In-situ TEM; Mo; Helium Implantation

I. INTRODUCTION

Exposure to hydrogen (H) and its isotopes directly affects the structural integrity of many materials. In some environments, helium (He) and its isotopes may also be encountered, in which case changes in microstructure and ultimately properties involve the combined effects of the two species. For instance, radioactive decay of tritium (T) produces helium-3 (^{3}He) within materials used for the solid-state storage and transport of T. Alternatively, H and He isotopes are implanted directly, or created as fission products by incident neutrons in some nuclear reactor applications. Whether arriving by decay or irradiation, these gas species may agglomerate in bubbles or cavities which adversely affect mechanical properties.[1] (In this paper, the term "bubble" consistently refers to volumes composed of gas only, and hence fully pressurized. In contrast, the term "cavity" refers to reduced-pressure volumes of vacancies and gas.) The processes governing cavity evolution are complex, and have been the focus of 50 years of work.[2-5]

Both natural aging and *ex situ* ion implantation have been used to study cavity formation in a range of metals.[2-4] In the latter, deuterium (D) and ^{4}He often act as surrogates for T and ^{3}He, respectively, as the structural differences between materials containing D or T are typically small,[6] and ^{4}He often behaves similarly to ^{3}He in terms of its effects on the microstructure. Here we use *in situ* transmission electron microscopy (TEM) techniques in an effort to provide a more fundamental understanding of cavity formation and growth in molybdenum (Mo) with and without prior exposure to gaseous D. Mo samples were subjected to ion irradiation *in situ* in the TEM, followed by brief room temperature aging, and finally heating *in situ* in the TEM. Cavity formation appears to be affected both by implanted ^{4}He and vacancies produced during

irradiation. This study provides a framework for quickly investigating microstructural processes that contribute to cavity formation in hydrogen isotope-bearing metals.

II. EXPERIMENTAL METHODS

Cross rolled Mo sheets were exposed to neutral D gas at elevated temperatures, and TEM samples were subsequently prepared by a lift-out technique using an FEI DB-235 dual beam focused ion beam/scanning electron microscope (FIB/SEM). The pristine and deuterated samples were finished with a low-kV polish,[7] and had final thicknesses of nominally 100 nm. The samples were then placed on the same carbon coated Cu TEM grid, ensuring near-identical implantation conditions. SRIM (Stopping and Range of Ions in Matter) simulations were performed with the SRIM-2013 software package,[8] utilizing 10 keV $^4He^+$ ions at an angle of 60° relative to the normal (similar to the experimental conditions).[9] Damage simulations using at least 25,000 $^4He^+$ ions were performed according to the guidelines suggested by Stoller, *et al.*, (Ref. 10) with a displacement energy of 65 eV.[11] The D concentration within the Mo resulting from gas exposure was expected to be dilute and was therefore not included in the simulations. *In situ* ion implantation with 10 keV $^4He^+$ was performed at room temperature at a rate of 2.9×10^{13} ions $cm^{-2}s^{-1}$ using the *In Situ* Ion Irradiation Transmission Electron Microscopy (I^3TEM) facility at Sandia National Laboratories.[9] Implantation was paused at 1, 10, and 100 minutes, corresponding to nominal fluences of 1.7×10^{15}, 10^{16}, and 10^{17} $^4He^+$ ions cm^{-2}, and still micrographs were collected to complement video recorded at 15 frames per second. Samples were aged at ambient lab conditions for one week prior to *in situ* annealing at an initial heating rate of 39 K min^{-1} to a nominal temperature of 1063 K with a Gatan heating stage in a Philips CM30 TEM. Post-annealing imaging was performed using an FEI Tecnai F30 TEM with both

bright field- and high-angle annular dark field scanning TEM (BF- and - HAADF-STEM) capabilities.

III. RESULTS AND DISCUSSION

SRIM simulations using a 100 nm-thick Mo target layer predicted that 37% of the $^{4}He^{+}$ ions were backscattered, 0.01% were transmitted, and 63% remained trapped within the layer, with the implanted ion distribution peak located approximately 30 nm beneath the surface. Since the 100 nm-thick layer represents the upper-bound estimate for TEM sample thickness, it is likely that the $^{4}He^{+}$ ion distribution peaks in the experiment were actually closer to the middle of the samples. The lack of transmitted ions also suggests that, to a first order approximation, the samples behave similarly to the surface region of a bulk sample.

Fig. 1a shows a triple junction in the D gas exposed Mo sample before $^{4}He^{+}$ implantation. After implantation to the lowest observed fluence of 1.7×10^{15} ions cm^{-2} (Fig. 1b), small round cavities were identified using Fresnel imaging (*i.e.* cavities appeared bright in under-focused conditions and inverted to dark when over-focused).[12] These cavities appeared both at grain boundaries and within grains, with diameters of approximately 0.5 nm. Increasing the fluence to 1.7×10^{16} and 10^{17} ions cm^{-2} (Fig. 1c) did not significantly change the cavity size. Cavity density was difficult to accurately quantify due to the large amount of strain contrast present. However, the density appeared to qualitatively increase.

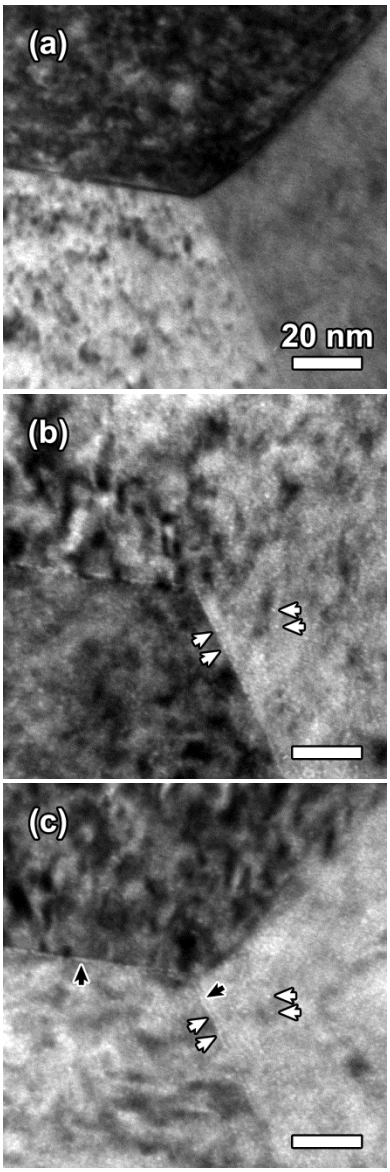

Fig. 1. Triple junction in D-exposed Mo (a) before implantation, (b) after 1.7×10^{15} and (c) 1.7×10^{17} $^4He^+$ cm^{-2}. Both (b) and (c) are under-focused to aid in cavity identification; cavities appear as light spots in these focus conditions. White arrows in (b) indicate cavities decorating a grain boundary, and another two within a grain. The white arrows in (c) show the same cavities as in (b), while black arrows note areas along grain boundaries that are now essentially strings of cavities. Note that the arrows explicitly point out only a few cavities for illustrative purposes. Many more cavities are visible in micrographs (b) and (c).

Previous studies using bulk Mo samples similarly found an increasing cavity density up to a critical dose of ~2×10^{17} ions cm^{-2} for He ions near 10 keV.[13] Such a fluence corresponds to

an extraordinary nominal concentration of implanted ^{4}He. Given the 63% retention percentage predicted by SRIM, the ^{4}He fluences reported here of 1.7×10^{15}, 10^{16}, and 10^{17} $^4He^+$ cm^{-2} correspond to nominal concentrations of 3.4×10^3, 10^4, and 10^5 atomic parts per million (appm) in Mo (calculated as $(\#_{He\ atoms})/(\#_{He\ atoms} + \#_{Mo\ atoms}) \times 10^6$). Despite the high concentration, cavity growth may be suppressed by a few factors. The high implanted ^{4}He concentration to displacements per atom (dpa) ratio is thought to promote local nucleation, and encourage the reintegration of He, inhibiting cavity growth and promoting finer cavity sizes.[14] In the present work, SRIM predicted a ^{4}He concentration to dpa ratio of approximately 5×10^4 appm ^{4}He dpa^{-1}. Furthermore, the actual He content remaining within the lattice is of some question. The concentrations computed above represent an upper-bound estimate, as SRIM does not consider the loss of implanted ions (*i.e.* due to diffusion back to the surface), which affect ^{4}He retention, especially in a thin TEM sample. Experimentally, ^{4}He concentrations in metals often saturate in the range of 10^3 to 10^4 appm during ion implantation.[5] Still, it is clear that enough He remained in the samples to create cavities.

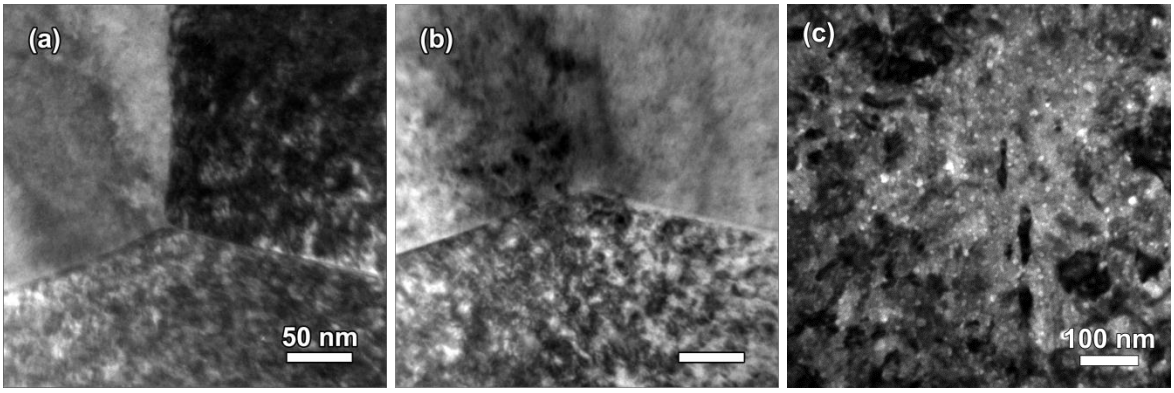

Fig. 2. Triple junction in unexposed Mo (a) as-lifted out and (b) after 1.7×10^{17} He^+ cm^{-2} (but prior to annealing). (c) Lower magnification under-focused image showing cavities in Mo after *in situ* annealing.

Microstructural changes during ^{4}He implantation and subsequent annealing were similar between pristine and deuterated Mo, as illustrated in Fig. 2a and b. The most notable difference was that the small cavities present in the D-exposed sample were not readily visible in the pristine sample after implantation. Some small black spots were found, suggesting the nucleation of small (< 0.5 nm) helium-vacancy (He-V) complexes or dislocation loops, as is expected during ^{4}He implantation at this energy.[14] The visible cavities observed in the implanted D-exposed Mo sample may have resulted from an impeded ability of the lattice to maintain ^{4}He in solution due to the presence of D.

Subsequent *in situ* heating experiments were performed to investigate the behavior of the small cavities that resulted from ^{4}He implantation. Few microstructural changes occurred until a nominal temperature of 1059 K was reached. At that point, larger cavities appeared over a period of a few seconds, and some cavity movement was noted. The series of snapshots in Fig. 3a-d shows the appearance and coalescence of two small cavities in the D-exposed Mo at a sustained nominal temperature of 1059 K. Here, the cavity in the center (white arrow) remains static as a reference point. Over several seconds, a number of other cavities appeared in the viewing area. A cavity just above the center (black arrow in 3b) first appeared, followed by a second cavity nearby (black arrow, 3c). The two cavities then joined, resulting in the larger cavity in 3d. Within a few minutes, the microstructure stabilized and no further changes were seen. After annealing, cavities tens of nm in diameter remained (Fig. 3e). However, higher magnification micrographs (Fig. 3f) revealed many smaller cavities on the order of a few nm remaining both within the grains and along a grain boundary. These features are similar to the cavities illustrated in Fig. 3a-d, but were distributed throughout the sample. It is not immediately clear why cavities in some

areas remained small, whereas larger agglomerations formed in other areas. This may be related to variations in the local microstructure.

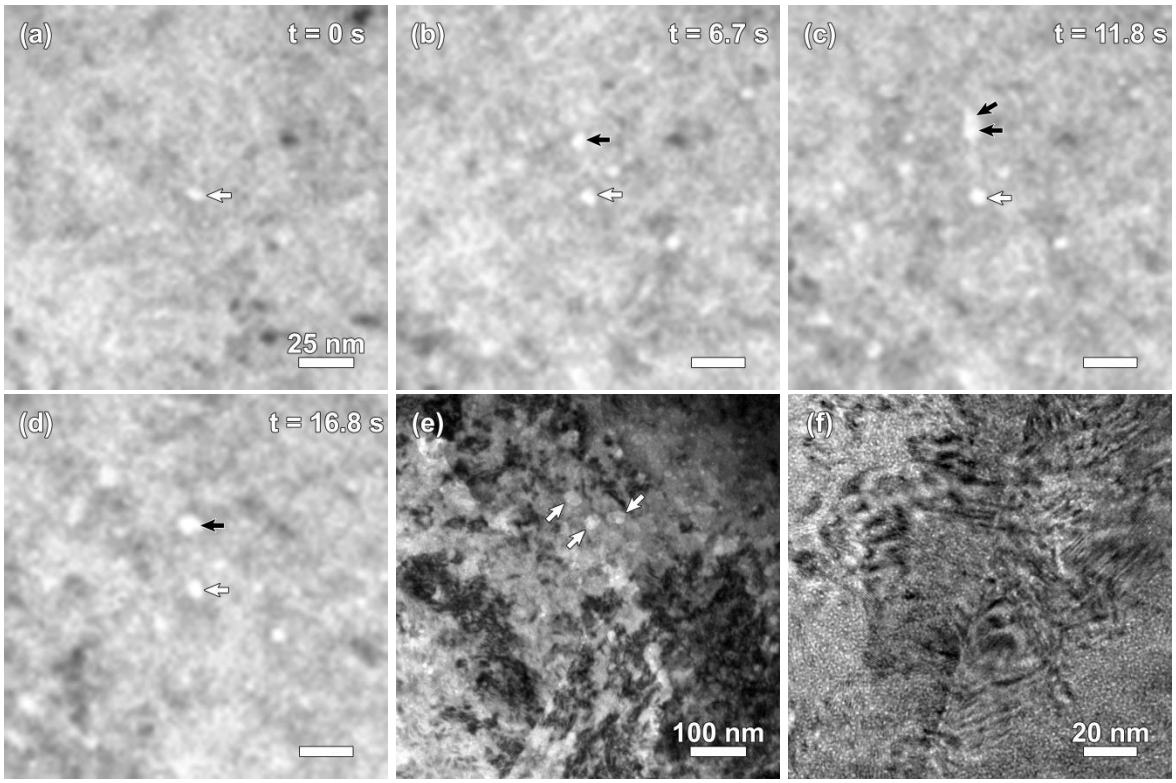

Fig. 3. (a-d) Cavity formation and growth in D-exposed Mo during *in situ* annealing at a nominal temperature of 1059 K. The white arrow indicates a static cavity. Black arrows indicate two cavities that appear, then merge in panels (b-d). (e,f) Low and higher magnification under-focused images of cavities in the same sample after annealing. Grain boundaries run through the middle of both (e) and (f).

The actual temperature of the samples during *in situ* annealing may have differed somewhat from the temperature recorded by the thermocouple attached to the heated boat due to thermal conductivity of through and between the Cu grid, C film and TEM sample itself. However, Erents and McCracken (Ref. 13) previously reported surface reorganization at 1100 K in Mo implanted with ^{4}He, followed by the release of most of the ^{4}He near 1400 K. The

coalescence of implanted ^{4}He into blisters and their subsequent rupture has been noted in a variety of metals.[15] *In situ* experiments are inherently influenced by the thin sample geometry, and should not be interpreted as full re-creations of the internal workings of bulk systems. However, such experiments still serve as a way to better elucidate mechanisms contributing to microstructural change. Hence, it is hypothesized that the observations in this study may help reveal the nanoscale mechanisms that drive the initial aspects of this blistering and rupture process.

Conventional TEM imaging identified the presence of cavities, but strain contrast obscured many other details of the microstructure, as is readily apparent in Figs. 2c and 3e. HAADF-STEM imaging techniques favor mass-thickness contrast by utilizing an annular detector to collect electrons scattered through large angles.[16] Electrons scattered through smaller angles by Bragg diffraction are excluded, and a result, contrast arising from local strain and bending is reduced. Hence, in the DF-STEM images in Figs. 4b and d, the cavities can be more clearly identified. These micrographs reveal that cavity size and shape varied nearly as much within each sample as it did between samples.

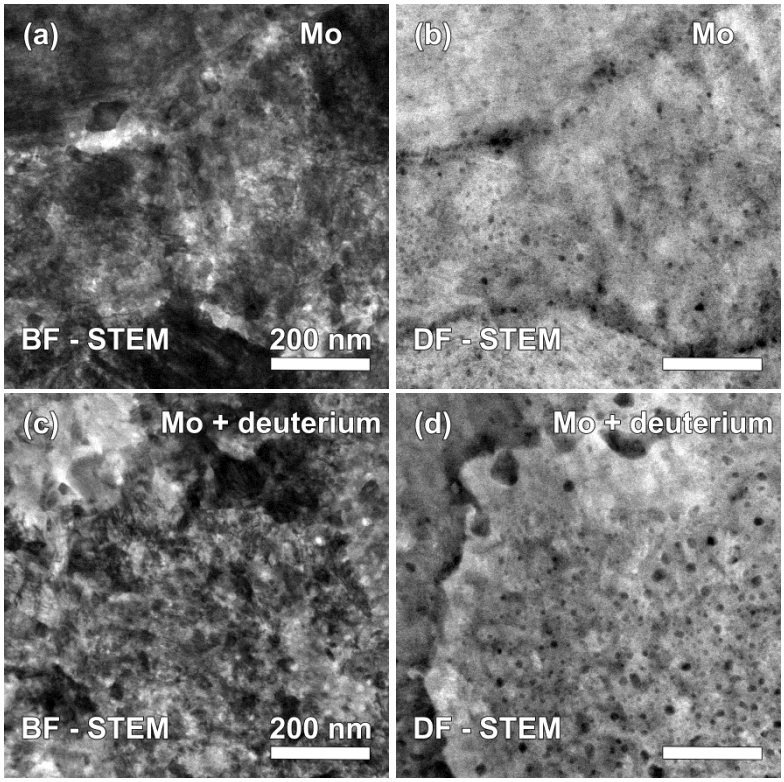

Fig. 4. BF- and HAADF-STEM images of pristine Mo (a,b) and D-exposed Mo (c,d) after implantation and annealing. Cavities are difficult to identify in the BF-STEM images in (a) and (c), however, the reduced strain contrast in the HAADF-STEM images (b) and (d) more clearly highlights the cavities, which appear as dark spots. Also note that in the HAADF-STEM images contrast is inverted from what is observed in BF imaging, *i.e.* thinner, lighter regions appear as darker, while thicker, heavier regions appear lighter.

The shapes of the cavities may provide some insight into the processes by which they were created. In equilibrium, an ideal spherical bubble has a pressure, p, of $-2\gamma/R$, where γ is the surface energy and R is the bubble radius.[1] As bubbles grow, they may remain spherical or evolve into crystallographically-oriented, plate-like shapes, depending on the surface energy and shear modulus.[17] These fully-pressurized conditions occur when gas arrives with minimal vacancy production, such as by T decay, where ^{3}He is produced with a recoil energy too low (0.35 eV) to cause lattice damage.[18] In the case of Mo, plate-like bubbles 1 nm-thick and 20 nm

in diameter have been observed after low energy (approximately 100 eV) implantations designed to minimize lattice damage.[2, 19]

The large cavities present after annealing were not plate-like, spherical, or faceted, but complex structure suggesting microstructural evolution processes involving vacancies generated during ^{4}He ion implantation dominated the cavity evolution. The simulated vacancy production during implantation was 6 vacancies ion^{-1}. As with implanted ions, SRIM accounts for defect generation, but not loss and recombination rates. Still, since the production bias favors vacancies,[20] it is reasonable to assume that vacancies would be available to combine with implanted ^{4}He. Incorporating vacancies would lower the pressure of the cavities, which would alter the driving force for plate-like or spherical bubbles. The local grain and dislocation structures may affect the retention of ^{4}He. Work by Buters, et al. (Ref. 21), indicated that the presence of dislocations from cold-working affected bubble formation in Mo. Also, grain boundaries vary in their ability to absorb point defects (sink strength),[22] and their ability to accommodate insoluble gas species.[23] Despite these factors, enough ^{4}He and vacancies clearly remained within the lattice to form large cavities during annealing after a week of aging at ambient conditions. The similar post-annealing microstructures between pristine and deuterated Mo suggest a common mechanism governing cavity formation that is not substantially affected by dilute D interstitials remaining from neutral D exposure. Cavity formation is generally not desirable for structural materials, as cavities often lead to swelling and a loss of ductility.[1] Fast diffusion of gas species back to surfaces may minimize the accumulation of gas within the lattice, provided it is implanted close enough to the surface. This may be a way to manage the accumulation of H in tungsten (W) in proposed fusion reactors.[24] Even so, accumulation of gas species at trapping sites may lead to undesirable structural evolution over time (*i.e.* "fuzz"

formation or blistering), especially in materials facing high fluxes simultaneously of incident neutrons, H, and He.[25]

A more complete understanding of the roles of microstructural defects (induced by both the material processing and radiation conditions) in the cavity formation and coalescence process might be realized by a more comprehensive set of experiments beyond the scope of the preliminary work presented in this paper. Although not explored here, the experimental parameters (including ion energies, ion species, ion fluxes, and total fluences) can be varied substantially. As discussed, the irradiation conditions in this study result in substantial amounts of displacement damage relative to the number of implanted ^{4}He ions. In contrast, more energetic ions that pass through the sample could be used to study the behavior of He-free voids, while implantation of sub-threshold displacement energy ^{4}He ions could be performed to study vacancy free bubble formation (as is the case with decay of T into ^{3}He). It bears mentioning that Mo often behaves similarly to W in many respects,[26] so similar studies might be used to better understand W materials in these complex environments.

IV. CONCLUSIONS

In situ ^{4}He ion implantation of Mo with and without prior D exposure was performed to a fluence of 1.7×10^{17} cm^{-2}. Small cavities were first noted at a fluence of 1.7×10^{15} ions cm^{-2}. These cavities increased in density, but not size, as fluence increased by two orders of magnitude. Post-implantation annealing to a maximum nominal temperature of 1059 K caused growth and agglomeration of these cavities, an observation that may be related to surface blistering in similarly treated bulk materials. Final cavity shapes were neither spherical nor crystallographically oriented, suggesting the incorporation of implanted ^{4}He and vacancies created by the implantation process. The combination of ion implantation and annealing

performed *in situ* inside of a TEM represents a powerful method for studying the mechanisms governing cavity evolution in Mo, with potential applicability to other material systems of interest for use in complex radiation environments.

V. ACKNOWLEDGEMENTS

The authors thank D. Buller, J. Desko, B. Doyle, M. Rye, and W. Wampler (Sandia National Laboratories) for their advice and assistance. This work was performed, in part, at the Center for Integrated Nanotechnologies, an Office of Science User Facility operated for the U.S. Department of Energy (DOE) Office of Science. Sandia National Laboratories is a multi-program laboratory managed and operated by Sandia Corporation, a wholly owned subsidiary of Lockheed Martin Corporation, for the U.S. Department of Energy's National Nuclear Security Administration under contract DE-AC04-94AL85000.

VI. REFERENCES

1. G. S. WAS, *Fundamentals of Radiation Materials Science: Metals and Alloys*. p. 416, Springer: New York, New York (2007).
2. S. E. DONNELLY, "The Density and Pressure of Helium in Bubbles in Implanted Metals: A Critical Review," *Radiat. Eff. Defect S.*, **90**, *1-2*, 1 (1985**)**.
3. H. TRINKAUS and B. N. SINGH, "Helium Accumulation in Metals During Irradiation - Where Do We Stand?," *J. Nucl. Mater.*, **323**, *2-3*, 229 (2003**)**.
4. S. J. ZINKLE and G. S. WAS, "Materials Challenges in Nuclear Energy," *Acta Mater.*, **61**, *3*, 735 (2013**)**.
5. C. S. SNOW et al., "He-3 Bubble Evolution in ErT_2: A Survey of Experimental Results," *J. Nucl. Mater.*, **453**, *1-3*, 296 (2014**)**.
6. M. A. RODRIGUEZ et al., "Unit Cell Expansion in ErT_2 Films," *Powder Diffr.*, **22**, *2*, 118 (2007**)**.
7. C. M. PARISH et al., "Processing Effects on Microstructure in Er and ErD_2 Thin-Films," *J. Nucl. Mater.*, **403**, *1-3*, 191 (2010**)**.
8. J. F. ZIEGLER et al., "SRIM - the Stopping and Range of Ions in Matter (2010)," *Nucl. Instrum. Methods Phys. Res. Sect. B*, **268**, *11-12*, 1818 (2010**)**.
9. K. HATTAR et al., "Concurrent in Situ Ion Irradiation Transmission Electron Microscope," *Nucl. Instrum. Methods Phys. Res. Sect. B*, **338**, 56 (2014**)**.
10. R. E. STOLLER et al., "On the Use of SRIM for Computing Radiation Damage Exposure," *Nucl. Instrum. Methods Phys. Res. Sect. B*, **310**, 75 (2013**)**.
11. C. E. KLABUNDE and R. R. COLTMAN, "Fission Neutron Damage Rates and Efficiencies in Several Metals," *J. Nucl. Mater.*, **108**, *1-2*, 183 (1982**)**.
12. J. W. EDINGTON, *Practical Electron Microscopy in Materials Science*. p. 175, Van Nostrand Reinhold Co.: New York, New York (1976).
13. S. ERENTS and G. M. MCCRACKEN, "Blistering of Molybdenum under Helium Ion Bombardment," *Radiat. Eff. Defect S.*, **18**, *3-4*, 191 (1973**)**.
14. N. M. GHONIEM, "Nucleation and Growth Theory of Cavity Evolution under Conditions of Cascade Damage and High Helium Generation," *J. Nucl. Mater.*, **174**, *2-3*, 168 (1990**)**.
15. O. AUCIELLO and R. KELLY, *Ion Bombardment Modification of Surfaces: Fundamentals and Applications*. pp. 11-22, Elsevier Science Publishers: New York, New York (1984).
16. D. B. WILLIAMS and C. B. CARTER, *Transmission Electron Microscopy: A Textbook for Materials Science*. pp. 376-386, Springer: New York, New York (2009).
17. D. F. COWGILL, "Physics of He Platelets in Metal Tritides," *Effects of Hydrogen on Materials*, 686 (2009**)**.
18. P. C. SOUERS, *Hydrogen Properties for Fusion Energy*. p. 212, University of California Press: Los Angeles, California (1986).
19. J. H. EVANS et al., "Direct Evidence for Helium Bubble-Growth in Molybdenum by the Mechanism of Loop Punching," *Scripta Metallurgica*, **15**, *3*, 323 (1981**)**.
20. H. TRINKAUS and H. ULLMAIER, "High-Temperature Embrittlement of Metals Due to Helium - Is the Lifetime Dominated by Cavity Growth or Crack-Growth?," *J. Nucl. Mater.*, **212**, 303 (1994**)**.
21. W. T. M. BUTERS et al., "A TEM Study of Helium Trapping in Cold-Worked Single Crystalline Molybdenum," *J. Nucl. Mater.*, **148**, *1*, 17 (1987**)**.

22. M. A. TSCHOPP et al., "Probing Grain Boundary Sink Strength at the Nanoscale: Energetics and Length Scales of Vacancy and Interstitial Absorption by Grain Boundaries in Alpha-Fe," *Phys. Rev. B,* **85**, *6*, 064108 (2012**)**.
23. M. RAJAGOPALAN et al., "Grain Boundary Segregation of Interstitial and Substitutional Impurity Atoms in Alpha-Iron," *JOM-US*, **66**, *1*, 129 (2014**)**.
24. J. ROTH and K. SCHMID, "Hydrogen in Tungsten as Plasma-Facing Material," *Phys. Scripta,* **2011**, *T145*, 014031 (2011**)**.
25. Y. UEDA et al., "Research Status and Issues of Tungsten Plasma Facing Materials for ITER and Beyond," *Fusion Eng. Des.,* **89**, *7-8*, 901 (2014**)**.
26. J. N. BROOKS et al., "Plasma-Facing Material Alternatives to Tungsten," *Nucl. Fusion,* **55**, *4*, 043002 (2015**)**.

FIGURE CAPTIONS

Fig. 1. Triple junction in D-exposed Mo (a) before implantation, (b) after 1.7×10^{15} and (c) 1.7×10^{17} $^4He^+$ cm^{-2}. Both (b) and (c) are under-focused to aid in cavity identification; cavities appear as light spots in these focus conditions. White arrows in (b) indicate cavities decorating a grain boundary, and another two within a grain. The white arrows in (c) show the same cavities as in (b), while black arrows note areas along grain boundaries that are now essentially strings of cavities. Note that the arrows explicitly point out only a few cavities for illustrative purposes. Many more cavities are visible in micrographs (b) and (c).

Fig. 2. Triple junction in unexposed Mo (a) as-lifted out and (b) after 1.7×10^{17} He^+ cm^{-2} (but prior to annealing). (c) Lower magnification under-focused image showing cavities in Mo after *in situ* annealing.

Fig. 3. (a-d) Cavity formation and growth in D-exposed Mo during *in situ* annealing at a nominal temperature of 1059 K. The white arrow indicates a static cavity. Black arrows indicate two cavities that appear, then merge in panels (b-d). (e,f) Low and higher magnification under-focused images of cavities in the same sample after annealing. Grain boundaries run through the middle of both (e) and (f).

Fig. 4. BF- and HAADF-STEM images of pristine Mo (a,b) and D-exposed Mo (c,d) after implantation and annealing. Cavities are difficult to identify in the BF-STEM images in (a) and (c), however, the reduced strain contrast in the HAADF-STEM images (b) and (d) more clearly highlights the cavities, which appear as dark spots. Also note that in the HAADF-STEM images

contrast is inverted from what is observed in BF imaging, *i.e.* thinner, lighter regions appear as darker, while thicker, heavier regions appear lighter.